



## Discover Generics

Cost-Effective CT & MRI Contrast Agents



FRESENIUS  
KABI

WATCH VIDEO

# AJNR

## Sodium MRI in Pediatric Brain Tumors



Aashim Bhatia, Cassie Kline, Peter J. Madsen, Michael J. Fisher, Fernando E. Boada and Timothy P.L. Roberts

*AJNR Am J Neuroradiol* published online 30 December 2024

<http://www.ajnr.org/content/early/2025/06/19/ajnr.A8642>

This information is current as  
of June 22, 2025.

# Sodium MRI in Pediatric Brain Tumors

 Aashim Bhatia, Cassie Kline, Peter J. Madsen, Michael J. Fisher, Fernando E. Boada, and  Timothy P.L. Roberts



## ABSTRACT

**SUMMARY:** Direct sodium MRI ( $^{23}\text{Na}$ -MRI) derives its signal from spin-manipulation of the  $^{23}\text{Na}$  nucleus itself and not the more conventional and familiar  $^1\text{H}$ -MRI. Although present at much lower concentrations in the human body than the  $^1\text{H}$  nuclei in the water molecule  $\text{H}_2\text{O}$ , advances in coil design and pulse sequence development have enabled the feasibility of human in vivo  $^{23}\text{Na}$ -MRI. Additionally,  $^{23}\text{Na}$ -MRI has the potential to offer nuanced physiologic insights not available to conventional MRI; this feature forms the basis of interest in its development and optimism for its novel clinical utility.  $^{23}\text{Na}$ -MRI has the potential to be a useful noninvasive imaging technique to assess biochemical and physiologic cellular changes in tissues, eg, cell integrity and tissue viability. Pathologically, the concentration of total sodium is elevated in tumors relative to normal counterparts due to increased intracellular sodium and/or an increased proportion of extracellular space (reflecting changes in cell morphology and anomalies of homeostasis). Here we review the technological advancements with improved pulse sequences and reconstruction methods that counter the inherent challenges of measuring sodium concentrations in the pediatric brain (in particular, its short-tissue T2 value) and present detailed imaging approaches to quantifying sodium concentrations in the pediatric brain that can be assessed in various CNS pathologies, with the focus on pediatric brain tumors.

**ABBREVIATIONS:** BSC = bound sodium concentration; IBR = iterative Bowsher reconstruction; IR = inversion recovery; ISC = intracellular sodium concentration;  $^{23}\text{Na}$ -MRI = sodium MRI; RF = radiofrequency; TPI = twisted projection imaging; TSC = total sodium concentration

Direct sodium MRI ( $^{23}\text{Na}$ -MRI) exploits similar atomic nuclear spin mechanisms that allow conventional proton ( $^1\text{H}$ ) MRI but derives its signal from manipulation of the  $^{23}\text{Na}$  nucleus itself.<sup>1,2</sup> Although present at much lower concentrations in the human body than the  $^1\text{H}$  nuclei in the water molecule  $\text{H}_2\text{O}$ , advances in coil design and pulse sequence development have enabled the feasibility of human in vivo  $^{23}\text{Na}$ -MRI. This uses the same MR scanner as conventional MRI (though it must be equipped with “heteronuclear” capability, primarily a broadband radiofrequency [RF] system, since the Larmor frequency of the  $^{23}\text{Na}$  spins differs from that of  $^1\text{H}$  protons). For the same reason, a dedicated transmit/receive RF coil is required; however, these are now commercially available for use at both 3T and 7T. While

conventional pulse sequences (eg, gradient-recalled echo) can often be manipulated to function at the resonance frequency of sodium, 33.8 MHz at 3T, instead of the conventional 127.1 MHz for  $^1\text{H}$  (based on the gyromagnetic ratios of sodium and hydrogen), dedicated pulse sequences are often preferred and will be discussed below. Given the challenges with sensitivity, coil hardware, and pulse sequence requirements, the adoption of  $^{23}\text{Na}$ -MRI might present some initial challenges. However, it has the potential to offer nuanced physiologic insights not available to conventional MRI, which form the basis of interest in its development and optimism for its novel clinical utility.  $^{23}\text{Na}$ -MRI has the potential to be a useful noninvasive imaging technique to assess biochemical and physiologic cellular changes in tissues, eg, cell integrity and tissue viability.<sup>3,4</sup>


$^{23}\text{Na}$ -MRI has demonstrated such potential in the pathophysiologic evaluation of acute ischemic stroke, multiple sclerosis, amyotrophic lateral sclerosis, migraines, and multiple tumor types, including tumors both within and outside of the CNS.<sup>3,5-11</sup> There is no radiation exposure with MRI (including  $^{23}\text{Na}$ -MRI), and  $^{23}\text{Na}$ -MRI does not use gadolinium-based contrast agents, eliminating the potential long-term risks of these agents commonly used in  $^1\text{H}$ -MRI; nor does it, in fact, rely on any other exogenous tracer (in contrast to PET, for example). The sensitivity of direct sodium imaging in detecting disease states stems from the tightly controlled  $\text{Na}^+$  ion homeostasis in healthy tissues, which

Received October 1, 2024; accepted after revision December 6.

From the Department of Radiology (A.B., T.P.L.R.), Division of Oncology (C.K., M.J.F.), and Division of Neurosurgery (P.J.M.), Children's Hospital of Philadelphia, Philadelphia, Pennsylvania; and Radiological Sciences Laboratory (F.E.B.), School of Medicine, Stanford, California.

This work was supported by an American Brain Tumor Association Discovery Grant, Society of Pediatric Radiology Pilot Grant, Department of Defense Exploration Grant.

Please address correspondence to Aashim Bhatia, MD, 3500 Civic Center Blvd, 2nd Floor, Office 2592 Philadelphia, PA 19104; e-mail: aashimbhatia@gmail.com; @draash

 Indicates open access to non-subscribers at [www.ajnr.org](http://www.ajnr.org)

 Indicates article with supplemental data.

<http://dx.doi.org/10.3174/ajnr.A8642>

maintains a large concentration gradient between intracellular sodium concentration (ISC) at 10–15 mmol/L and extracellular sodium at ~145 mmol/L. The concentration of total sodium is elevated in tumor cells relative to normal tissues due to increased intracellular sodium concentration and/or an increased proportion of extracellular space (reflecting changes in cell morphology).<sup>8</sup>

In neoplastic tissue, sustained depolarization of the cell membrane with altered  $\text{Na}^+/\text{H}^+$  pump transport kinetics precedes the high rate of mitotic activity that characterizes abnormal tumor growth, leading to a concomitant increase in the ISC that has been demonstrated in a number of human neoplasms (Supplemental Data).<sup>12–14</sup> Further characterization of this rise in intracellular sodium concentration in several types of human carcinomas and glial cell lines has established a positive correlation between proliferative activity and an increased intracellular  $\text{Na}^+:\text{K}^+$  ratio (mostly due to an increase in ISC). An increase in ISC contributes to an increase in total sodium concentration (TSC). Research suggests that elevated abnormal changes in voltage-gated sodium channels ( $\text{Na}_v1.3$ ,  $\text{Na}_v1.6$ ) in low-grade astrocytomas and increased expression of the Na, K-ATPase  $\beta$ -subunit isoforms in peritumoral astrocytes may contribute to the increases in both ISC and TSC.<sup>15</sup> In addition, pediatric brain tumor tissues consist of up to 30% non-neoplastic cells, including glioma-associated microglia, monocyte-derived macrophages, myeloid-derived suppressor cells, and tumor-infiltrating  $\text{CD4}^+$  and  $\text{CD8}^+$  T-cells.<sup>16</sup> The tumor microenvironment is similarly characterized by low glucose, low oxygen, and high acidity, resulting from aerobic glycolysis (Warburg effect) in highly proliferative cancer cells to meet their high nutrient demand, despite the presence of oxygen and fully functioning mitochondria.<sup>17,18</sup> Activation of other  $\text{Na}^+$  ion transport proteins (such as  $\text{H}^+$  extrusion protein  $\text{Na}^+/\text{H}^+$  pump and cell volume regulatory protein Na-K-Cl pumps) could also contribute to increased ISC and TSC in tumor tissues, which have been detected in glioma cells as well as in glioma-associated microglia and peritumoral reactive astrocytes.<sup>19</sup> Changes of  $\text{Na}^+$  transport protein expression and function in tumor cells, tumor-associated glial cells, and tumor infiltrating immune cells play a role in the elevated sodium concentrations in pediatric brain tumors.<sup>20</sup> Thus, direct sodium imaging with  $^{23}\text{Na}$ -MRI offers attractive sensitivity to the processes of the cell membrane.

There have been promising results suggesting that sodium levels can predict CNS tumor types and even predict progression-free survival.<sup>11,21–23</sup>  $^{23}\text{Na}$ -MRI has been shown to be a marker of tumor proliferation in animal glioma models and, most important, has shown the ability to distinguish between posttreatment necrosis and treatment responses.<sup>22</sup> In adult (human) brain tumors,  $^{23}\text{Na}$ -MRI has demonstrated the ability to provide an additional marker for differentiating high-grade and low-grade

tumors, treatment response, and even determining a molecular mutation, with direct measurement of sodium concentrations complementary to  $^1\text{H}$ -MRI.<sup>11,13,21</sup> In a study of 20 adult patients with malignant brain tumors, the mean sodium concentration (in millimoles per kilogram wet weight) was 61 (SD, 8) for gray matter, 69 (SD, 10) for white matter, 135 (SD, 10) for CSF, 113 (SD, 14) for vitreous humor, and, most important, 103 (SD, 36) for brain tumor, which is significantly elevated compared with reference brain tissues.<sup>12</sup> Recently, we published the first report of application of  $^{23}\text{Na}$ -MRI to pediatric brain tumor imaging.<sup>13</sup>

Technical challenges in  $^{23}\text{Na}$ -MRI in the pediatric brain necessitate an optimized MRI sequence, for which there is currently no standard approach or consensus. This article will summarize the multiple technical factors and hardware involved in estimating sodium concentrations using  $^{23}\text{Na}$ -MRI in the pediatric brain, considering pulse sequences, RF coils, and reconstruction methods. In addition, incompletely appreciated physiology associated with sodium changes in the brain during myelination or even in neonates with relatively more incomplete myelination compared with older children present areas of interest in the research field as well as essential questions that need to be answered as a part of clinical implementation.

## Equipment

Details of the  $^{23}\text{Na}$ -MRI technique will be dependent on the MRI system and hardware available. A brief overview of hardware requirements will be necessary before discussing the  $^{23}\text{Na}$ -MRI technique. Sodium concentrations are 1000s of fold less than hydrogen protons in the human body, particularly in the human brain, where there is an average of 35–45 mmol/L of sodium ions compared with 80M proton concentration in the hydrogen nuclei of water molecules (Table).<sup>23</sup> Not only is the sodium ion concentration so much lower (compromising sensitivity), but the fundamental sensitivity of the nuclear magnetic resonance (NMR) experiment is intrinsically lower for the  $^{23}\text{Na}$  nucleus compared with  $^1\text{H}$ , being linearly dependent on the gyromagnetic ratio (which differs among nuclei and is approximately 25% for sodium compared with hydrogen). This finding compromises sensitivity (and, ultimately, SNR) further. Worse still, the T2-decay constants of sodium nuclei in vivo are very short (especially for the intracellular component—as low as ~3–5 ms at 3T), presenting a further challenge to signal detection, requiring very short TEs. These factors have generally led to a practical minimum field strength requirement of 3T to obtain adequate sodium signal. Additionally, because of the different Larmor frequency of sodium (approximately 33.8 MHz at 3T), the scanner will need to be equipped with a broadband RF system (sometimes called heteronuclear, or X-nucleus, package).

## Sensitivity of alternative nuclei in brain<sup>a</sup>

Nucleus	Gyromagnetic Ratio MHz/T	Scanner Frequency	Tissue Concentration	Relative NMR Sensitivity	Relative Biologic Sensitivity
$^1\text{H}$	42.58	127.1	88 mol/L	1	1
$^{23}\text{Na}$	11.26	33.8	35–45 mmol/L	0.092	~0.0001
$^{31}\text{P}$	17.24	51.7	1–10 mmol/L	0.0663	~0.00001
$^2\text{D}$	6.54	19.5	0	0.0000096	0
$^{19}\text{F}$	40.08	120.24	0	0.83	0

**Note:**—NMR indicates nuclear magnetic resonance.

<sup>a</sup> $^2\text{D}$  and  $^{19}\text{F}$  are tracer techniques, as endogenous tissue concentrations are zero. Clinically, only  $^{23}\text{Na}$  (and imaginably  $^{31}\text{P}$ ) provide sufficient in vivo sensitivity.

Since the US Food and Drug Administration (FDA) first approved the 3T system in 1999, research in  $^{23}\text{Na}$ -MRI has benefited from improved gradients and electronics to improving the clinical feasibility through shorter minimum TE values. Lower spatial resolution ( $\sim 3$  mm isotropic) is often an accepted compromise along with relatively long acquisition times ( $\sim 10$  minutes) due to the low SNR. SNR increases approximately linearly with increased field strengths (though T2 values may shorten further), and there are, thus, advantages of imaging at higher field strengths, namely 7T, which will be discussed below.

### Imaging Technique

TSC within the brain is a signal from both the extracellular and intracellular spaces. The extracellular space consists primarily of the interstitial space, which contains extracellular matrix and cells. Vascular (3% of volume) and perivascular spaces are also included in the extracellular space but occupy a much smaller percentage. The rapid  $^{23}\text{Na}$ -MRI signal loss, which was initially believed to be from primarily short-T2 intracellular compartments, is now considered reflective of both interstitial and intracellular spaces. Much interest is focused on resolving the intracellular and short-T2 component of the sodium signal, sometimes called the bound sodium concentration (BSC).

### Acquisition Approaches in $^{23}\text{Na}$ -MRI

Given intracellular sodium T2 values as short as  $\sim 3$ –5 ms compared with relatively longer (though still short) T2 values in the extracellular space ( $\sim 25$ –30 ms), conventional imaging sequences with relatively longer TEs will be preferentially sensitive to the extracellular and, even free-fluid, sodium signal only. Consequently, images acquired with conventional TEs  $> \sim 5$  ms tend to have the imaging characteristics of CSF maps, with relatively weak (if detectable) contribution from brain parenchyma.

Thus, ultra-short TEs ( $\sim 0.5$ –5 ms) are required to obtain signal from the rapidly decaying signal from sodium ions in the body (especially for sodium ions in the intracellular environment). Short-TE scanning can be achieved using some gradient-echo sequences; ultra-short TE scanning tends to use some variant of spiral or radial scanning (with signal sampling starting at or near the center of  $k$ -space) to maximize signal sensitivity.<sup>24–26</sup>

Even typically-used radial-scanning readout results in SNR loss and inefficient sampling of  $k$ -space. Optimized approaches to sampling  $k$ -space in  $^{23}\text{Na}$ -MRI have been developed, such as twisted projection imaging (TPI), which improves the SNR.<sup>27</sup> Ultra-short TE sequences acquire spin density-weighted  $^{23}\text{Na}$ -MRI (note these are  $^{23}\text{Na}$  spin density, and not “proton density”), which allows directly estimating sodium concentrations in tissues.

There is clinical interest in sodium concentrations that are reflective of the intracellular space, which can be more representative of pathologic diseases in children, such as in neoplasms, demyelinating disease (multiple sclerosis), and stroke.

Several strategies have been explored to suppress the relatively hyperintense  $^{23}\text{Na}$ -MRI signal from CSF (also, sometimes, necrosis) to emphasize relatively lower signal contributions from brain parenchyma. Inversion recovery (IR) (based on the difference in sodium T1 values) is an approach to attempt to suppress the sodium signal from the CSF; however, IR has not gained tremendous interest due

to the low SNR and limitations with specific absorption rate (SAR) due to 180° pulses.<sup>28</sup>

So-called dual echo sodium imaging has been performed in adults and children, in which 2 images are acquired (potentially in the same pulse sequence) at 2 different (but both short) TEs. The signal from these images is modeled, pixelwise, for a pool comprising 2 components. A simple linear equation then allows the separation of these component pools without incurring the SNR losses associated with the IR method, provided some mathematical assumptions are made. This approach allows a much greater SNR and lower SAR compared with IR, while still achieving  $^{23}\text{Na}$  fluid suppression. Since the dual-echo approach is essentially a subtraction technique, it is also vulnerable to differential sensitivity to magnetic susceptibility artifacts, leading to erroneous elevated signal on subtraction in regions of bone-tissue or air-tissue interface, which may masquerade as fluid-suppressed tissue sodium signal.<sup>27</sup>

To illustrate the dual-echo approach with corresponding mathematics, we describe a simplified model formulation (after Qian et al, 2015):<sup>27</sup>

Consider a simple 2-compartment model, consisting of 1 fraction  $a_F$  in a “free” environment, characterized by the T2-decay constant  $T_{2F}$  and a second (“tissue”) fraction ( $= 1 - a_F$ ) characterized by a different T2-decay constant,  $T_{2T}$ .

$$\text{FREE} : \alpha_F, T_{2F} \quad \text{TISSUE} (1 - \alpha_F), T_{2T}.$$

The observed sodium signal  $S$ , for a pulse sequence with TE, will be an average over the 2 pools (weighted by compartment volume fraction and T2 values):

$$S = S_0 \cdot \{ \alpha_F \cdot \exp(-TE/T_{2F}) + (1 - \alpha_F) \cdot \exp(-TE/T_{2T}) \},$$

noting that  $T_{2F}$  is relatively longer and  $T_{2T}$  is shorter. So, for 2 imaging pulse sequences with TEs 0.5 and 5 ms respectively:

$$\begin{aligned} \text{Short TE} : S(0.5) = S_0 \cdot \{ \alpha_F \cdot \exp(-0.5/T_{2F}) \\ + (1 - \alpha_F) \cdot \exp(-0.5/T_{2T}) \}, \end{aligned}$$

$$\begin{aligned} \text{Long TE} : S(5.0) = S_0 \cdot \{ \alpha_F \cdot \exp(-5/T_{2F}) \\ + (1 - \alpha_F) \cdot \exp(-5/T_{2T}) \}. \end{aligned}$$

Simple Subtraction (since the free component is relatively bright on both)

$$\begin{aligned} S(0.5) - S(5.0) \sim S_0 \cdot \{ (1 - \alpha_F) \cdot [\exp(-0.5/T_{2T}) \\ - \exp(-5/T_{2T})] \} \end{aligned}$$

$$\sim S_0 \cdot \{ (1 - \alpha_F) \cdot [\exp(-0.5/T_{2T}) - 0] \} \text{ if } T_{2T} < 5 \text{ ms}$$

$$\sim S_0(1 - \alpha_F), \text{ if } T_{2T} > 0.5 \text{ ms},$$

suggesting the so-called “short T2 image,” formed by simple subtraction, yields a signal proportional to the tissue fraction of sodium  $\alpha_T = (1 - \alpha_F)$ .

In practice, this simple subtraction fails to completely suppress longer T2 species, since the assumption that

$$\{\alpha_F \cdot \exp(-0.5/T_{2F})\} - \{\alpha_F \cdot \exp(-5/T_{2F})\} \sim 0,$$

is not met exactly for realistic values of  $T_{2F}$ . Consequently, we propose a weighted subtraction better suited for nulling of long  $T_{2F}$  species (eg, the fluid hyperintensities that obscure the conspicuity of pathology in the in vivo brain). Consider a weighting factor,  $\beta$ , (where  $\beta$  is approximately 15%):

Weighted Subtraction:

$$\begin{aligned} "S(0.5) - (1 + \beta)S(5.0)" \sim \text{So. } \{ & (1 - \alpha_F) \cdot [\exp(-0.5/T_{2T}) \\ & - (1 + \beta)\exp(-5/T_{2T})] \}. \end{aligned}$$

In this case, the free compartment has much reduced residual signal since the assumption,

$$\{\alpha_F \cdot \exp(-0.5/T_{2F})\} - (1 + \beta) \{\alpha_F \cdot \exp(-5/T_{2F})\} \sim 0,$$

does indeed hold; thus, the weighted subtraction image yields signal proportional to the tissue sodium fraction alone. The factor,  $\beta$ , needed to allow complete subtraction of the free pool signal depending on the T2 value of that fraction ( $T_{2F}$ ) and on the 2 chosen TEs. It can be determined empirically (during postprocessing) or estimated on the basis of the literature  $T_{2F}$  values. Thus, the weighted subtraction can be considered to reflect the tissue sodium fraction (weighted only by  $T_{2T}$  values). Illustrations of this methodology throughout this article will use a  $\beta = 15\%$  as an exemplar. Note, as with all subtraction techniques, but especially with those with relatively longer acquisition times (approximately 10 minutes), misregistration of the 2 image sets can lead to subtraction artifacts. A pulse sequence with interleaved TEs could be created or reregistration could be facilitated with the use of sodium chloride solution fiducials analogous to the commonly used vitamin E capsules for navigation sequences, to combat this outcome.

In reality, even the cellular (non-“free”) pool may itself be multicompartmental. This possibility leads to either a higher-order multicompartmental approach or at least a hierarchical multistep, 2-compartment model, likely necessitating further image acquisitions (with different TE choices). Such multicompartment models have been used to attempt to separate intracellular sodium from extracellular sodium concentrations. Combining fluid-suppressed IR and spin density-weighted imaging has also been used to estimate the pseudo-intracellular sodium concentration and extracellular volume fraction. The reliability of such a 3-compartment model has been challenged due to disease-related fluctuations in the parameters whose values are fixed by assumption: fixed relaxation times, fixed intracellular sodium concentration, and fixed volume fractions. Others have suggested a fourth compartment, myelin water, which contains equal ratios of intracellular and extracellular sodium.<sup>29</sup> The further expansion of differentiating the sodium signal into 3 or even possibly 4 compartments may, thus, be needed to improve the accuracy of the representation of the sodium physicochemical microenvironment. Nonetheless, the 2-compartment approach offers promise for ready clinical adoption.

At this point, the alternative strategies for sodium quantification based on triple quantum filtering may indeed offer more precise specificity but at the price of both SNR as well as analysis complexity and are considered beyond the scope of current clinical implementation.

### Localized T2\* Mapping Schemes

T2\* measured at multiple TEs has the potential to measure sodium concentrations in different molecular environments. Localized T2\* mapping can take a long time, but if it is combined with optimized multiecho readout schemes (3D MERINA), the acquisition times can be decreased.<sup>30</sup> Furthermore, local T2\* mapping may also provide a practical basis for improving the local image blurring associated with T2\*-dependent decay of signal along the spiral (or other)  $k$ -space trajectory.

Other factors in the correction of relaxation effects include TEs desired, which cannot be obtained due to hardware limitations, switching times between transmit and receive channels of the RF coil, or SAR limitations restricting the minimum pulse duration (because of its high peak  $B_1$  amplitude and, thus, RF power), and in certain tissues with very short transverse relaxation times, this leads to signal loss from T2\* relaxation. In the clinical setting, short TRs that do not allow complete longitudinal relaxation (<100 ms) are sometimes used. Such short TRs can lead to biases in the estimation of the tissue sodium concentration. If the T1 and T2\* relaxation times are known or can be reasonably estimated, relaxation effects can be corrected by calculating the relaxation-correction factors for mono and biexponential relaxation.

### Advanced Imaging Reconstruction

There are multiple approaches to image reconstructions to decrease the rather long acquisition times of  $^{23}\text{Na}$ -MRIs and/or improve the relatively low resolution. Radial and spiral acquisitions commonly used in  $^{23}\text{Na}$ -MRI can take advantage of compressed sensing for iterative reconstruction. With the increasing implementation of deep learning-based reconstruction algorithms in  $^1\text{H}$ -MRI, analogous optimization of  $^{23}\text{Na}$ -MRI is to be expected. However, the greater the degree of “actual” undersampling, the greater is the possibility of inaccurate estimation of the true sodium concentrations, which has been shown in prior studies.<sup>31</sup>

$^1\text{H}$ -MRI provides high-resolution, low-noise anatomic detail that can be combined with  $^{23}\text{Na}$ -MRI. Beyond simple overlay (as in eg, fMRI), this result might best be approached with a constrained reconstruction approach. This method considers the possibility of losing important sodium data, and only shared data between  $^1\text{H}$ - and  $^{23}\text{Na}$ -MRI are interpreted. This reconstruction approach allows improved resolution and low-noise sodium images with greater contrast between gray matter and white matter.<sup>32</sup> One emerging technique is the iterative Bowsher reconstruction (IBR) framework, which essentially deconvolves spatial T2-blurring using a T2 estimate from 2 TEs and anatomic priors from high-resolution T1-weighted or FLAIR images (Fig 1).<sup>32</sup> This method is widely used in sharpening PET images and has been adapted to  $^{23}\text{Na}$ -MRI. The proton MRI is coregistered with the  $^{23}\text{Na}$  MR images to confirm the location of brain tumors.



**Clinical Implementation Vignette.** We illustrate the above concepts with a specific and detailed example of a patient with a diffuse midline glioma of the pons. In the sodium MR imaging acquisition,  $^{23}\text{Na}$ -MR images were acquired on a 3T scanner (Magnetom Prisma; Siemens), equipped with heteronuclear capabilities; the RF coil for  $^{23}\text{Na}$  is a dual-tuned ( $^1\text{H}$ - $^{23}\text{Na}$ ) head volume coil (Rapid MRI). A custom-developed pulse sequence, TPI, is used to acquire  $^{23}\text{Na}$ -MRI data for TSC and BSC imaging using a dual-TE technique ( $\sim 10$  minutes per sequence, total of  $\sim 20$  minutes to acquire both TEs), analogous to our prior work: field of view =

220 mm, matrix size =  $64 \times 64 \times 64$ , voxel size = 3.44 mm (isotropic),  $\text{TE}_1/\text{TE}_2 = 0.5/5$  ms,  $\text{TR} = 100$  ms, averages = 4, and Time to Acquisition (TA) = 10 minutes, 38 seconds for each TE.

**TPI and Dual-Echo-Based Reconstruction.** The dual-echo TPI approach to measure BSC allows both an optimized ultra-short TE (as low as 0.3 ms) acquisition as well as a deblurred image reconstruction based on  $\text{T}2^*$  fitting, rendering higher-quality reconstructed images (with reduced  $\text{T}2^*$ -blurring). The ultra-short TE is achieved via asymmetric sampling of projection imaging with radiations from the center of the  $k$ -space along the polar and azimuthal angles. The TE is only limited by the RF excitation pulse and the associated rephasing gradient in case of slice selection. The dual-TE  $^{23}\text{Na}$ -MRI allows suppression of the elevated “free” sodium signal within both CSF and necrotic foci, resulting in improved distinction of non-neoplastic from neoplastic tissue. In the examples below (Figs 2–3), we use the 115%-weighted subtraction described above to optimize free fluid sodium suppression.

The dual-TE  $^{23}\text{Na}$ -MRI allows suppression of the elevated “free” sodium signal within both CSF and necrotic foci, resulting in improved distinction of non-neoplastic from neoplastic tissue. In the examples below (Figs 2–3), we use the 115%-weighted subtraction described above to optimize free fluid sodium suppression.

#### **$^{23}\text{Na}$ Image Reconstruction: Postprocessing and Quantitative Sodium MR Imaging**

We have developed a postprocessing method that uses the intensity of  $\text{TE}_1$  to linearly calibrate using the CSF region ( $\text{TSC} = 145$  mmol/L) and noise-only background ( $\text{TSC} = 0$  mmol/L). Sodium images are registered to anatomic T1-weighted, T2-weighted, or FLAIR proton images using 6 *df* rigid body transformation in medical imaging processing, analysis, and visualization (MIPAV; (<https://mipav.cit.nih.gov/>) software (Fig 4).

Imaging reconstruction methods based on similar low-resolution PET and fMRI have been applied to  $^{23}\text{Na}$ -MRI with promising results. Incorporating

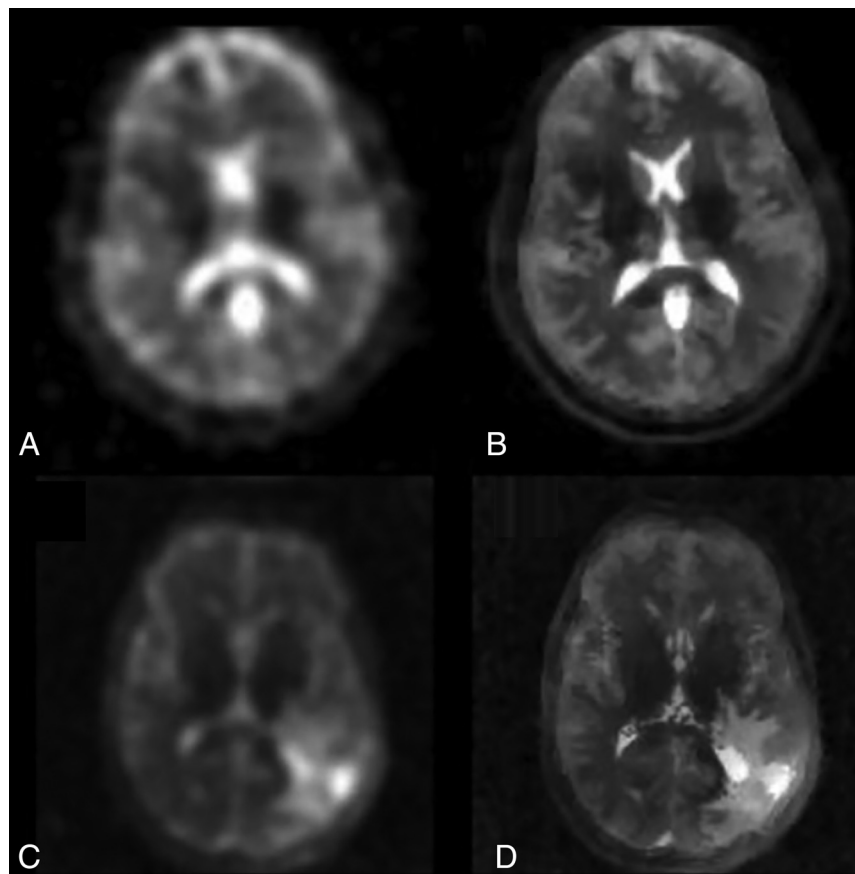


**FIG 1.** Deblurring  $^{23}\text{Na}$ -MRI with iterative Bowsher reconstruction. A, Native  $^{23}\text{Na}$ -MRI of a healthy volunteer (A) can be significantly sharpened to B using 2-point  $\text{T}2$  estimation and anatomic priors. Similarly, C and D demonstrate the benefit of IBR deblurring in a patient with glioma, allowing clearer intracranial resolution.

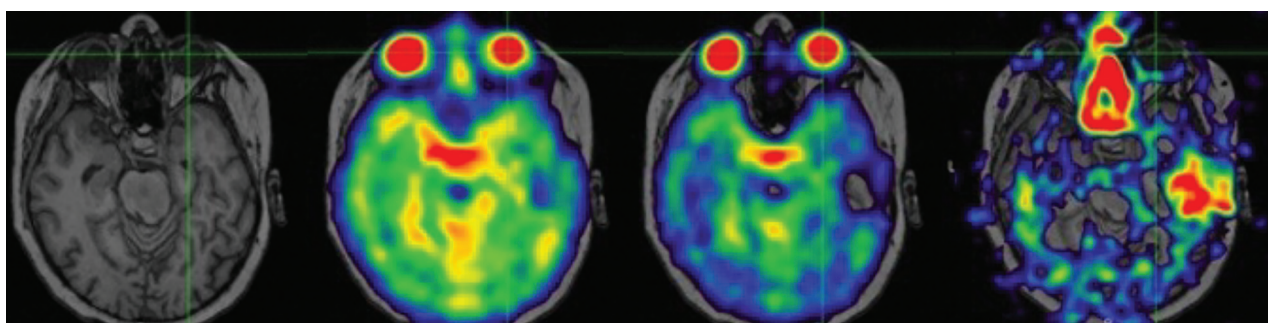


**FIG 2.** Dual-TE  $^{23}\text{Na}$ -MRI in a pediatric patient with suppression of the elevated “free” sodium signal within vitreous fluid of the globe (cross-hair). Note  $\text{T}2$ -based signal loss from  $\text{TE} = 0.5$ –5 ms. Also note, susceptibility artifacts in the left temporal lobe and nasal cavity, becoming especially pronounced on subtraction. (Same patient in Figs 3–6).

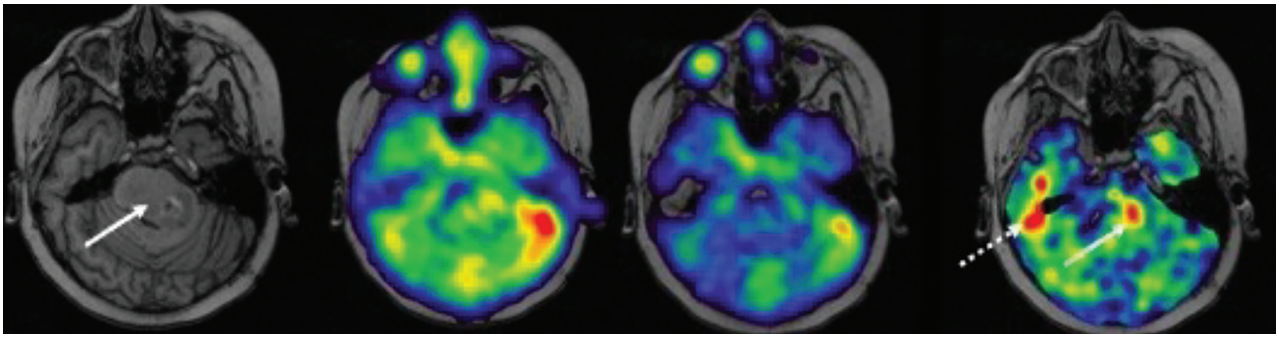


**FIG 3.** Diffuse midline glioma centered in the pons in a pediatric patient. T1 MPRAGE with tumor (solid arrow) centered in the pons extending into the left middle cerebellar peduncle. Subtraction of the 2 echo times demonstrates a focal region of elevated sodium in the tumor (arrow). Susceptibility artifact displays as elevated signal in the region of the right temporal bone (dashed arrow), which could potentially be misinterpreted as elevated tissue sodium concentration (same patient as above).

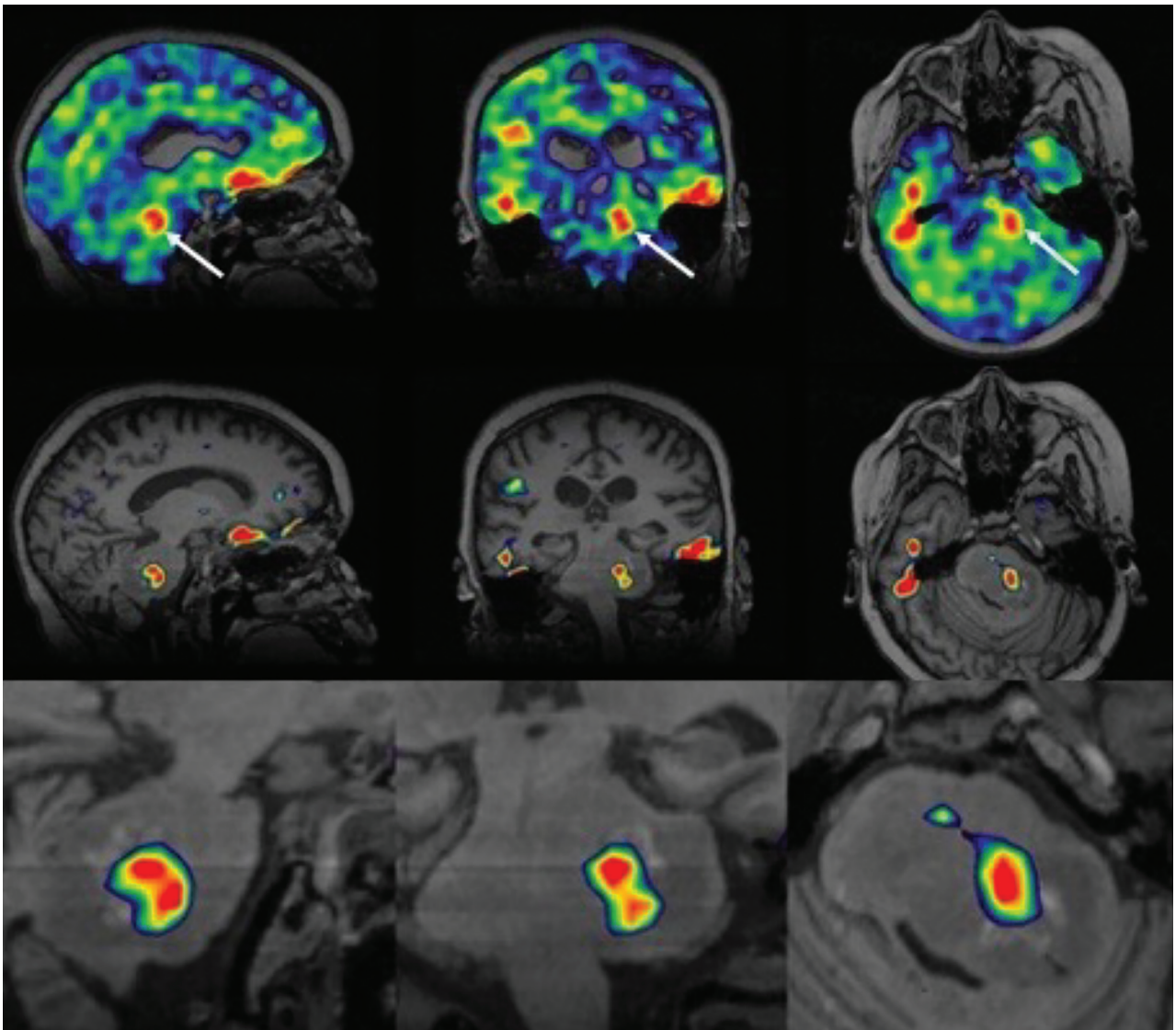


**FIG 4.** Thresholding the sodium concentrations in the pediatric patient above. Focal region of elevated sodium in the tumor (arrow). Thresholding allows precise depicting of the tumor.

anatomic prior insights from  $^1\text{H}$ -MRI allows anatomically-guided reconstruction, for example.<sup>32</sup> The TPI sequence that is relatively widely used offers  $\sim 3.4$ -mm isotropic resolution, somewhat

comparable with fMRI and, though justifiable in terms of its physiologic value, benefits from such anatomically-enhanced reconstruction.



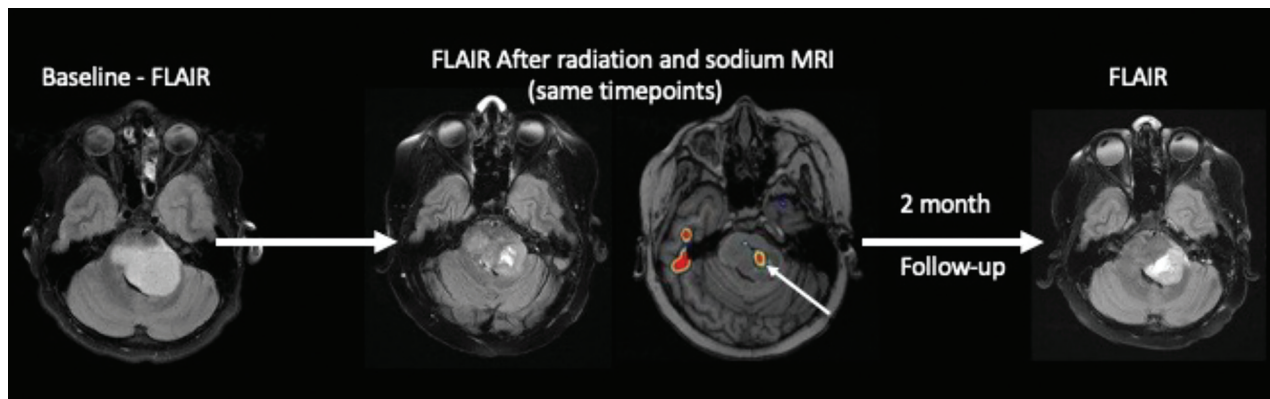


**FIG 5.** Pediatric patients with diffuse midline glioma from above. The increased focus of sodium concentrations (*arrow*) in the tumor was acquired after radiation treatment; this region may represent the following: radioresistant region of the tumor (A) and region of tumor progression (B). Follow-up conventional MRI a further 2 months after radiation cessation demonstrates tumor progression in the region of the prior sodium elevation. This anecdote supports the hypothesis that elevated sodium signal represents an early biomarker of tumor progression/recurrence.

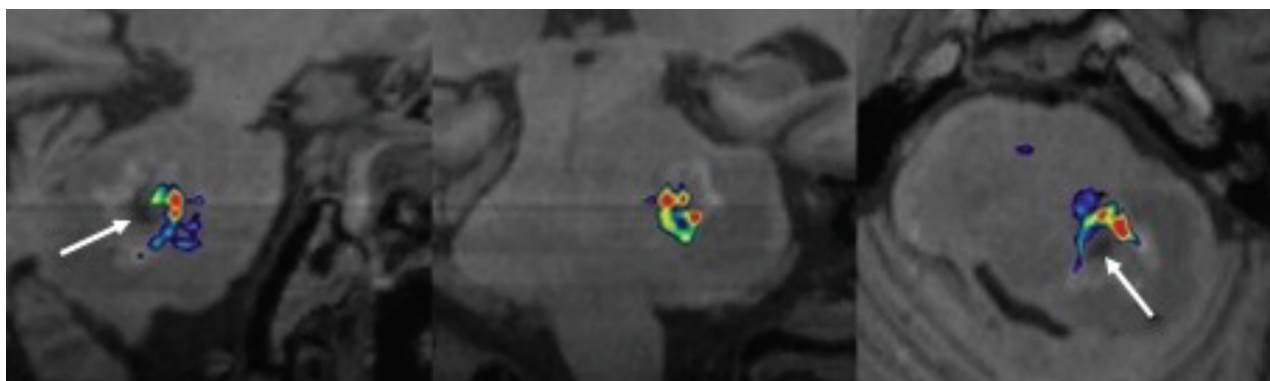


**FIG 6.** Using the T1-weighted sequence to further suppress necrotic regions (*arrows*) within the diffuse midline glioma (same patient as above) in a composite  $^1\text{H}$ -MRI and  $^{23}\text{Na}$ -MRI integration.

**Possible Clinical Utility.** Sodium MRI has the potential to be a more physiologically-specific imaging marker, compared with conventional  $^1\text{H}$ -MRI in determining treatment responses (Fig 5). Sodium MRI is sensitive to tumor recurrence that is not visualized on conventional  $^1\text{H}$ -MRI.<sup>33</sup> Thus,  $^{23}\text{Na}$ -MRI provides an objective imaging biomarker of tumor biologic activity.  $^{23}\text{Na}$  promises to offer a pivotal imaging finding in pediatric patients with brain tumors to allow neuro-oncologists the clear indication needed to modify treatment regimens, by providing a more definitive and physiologically-interpretable imaging marker of brain tumor progression and treatment efficacy.

**Future Directions.** High-field (7T) MRI allows technical advances in sodium imaging in the pediatric brain. The recent FDA-approved 7T Terra X magnet (Siemens) is equipped for heteronuclear imaging with a dual-frequency  $^{23}\text{Na}/^1\text{H}$  coil. 7T has advantages in sodium MRI such as decreasing image-acquisition time, improving SNR (approximately doubling that obtained at 3T), and thus increased resolution, though noting that increasing spatial resolution by a factor of 2 results in a decreased SNR by a factor of 8 if using a 3D isovolumetric sequence.<sup>23,34–37</sup> Thus, the potential 7T advantages must be tailored for the specific clinical question, such as in treatment of brain tumors, in which early

treatment effects can be better evaluated with  $^{23}\text{Na}$ -MRI due to improved SNR.

#### Multimodal T1-Weighted Enhancement of Sodium Images.

Figure 6 illustrates an interesting potential integration of  $^1\text{H}$ - and  $^{23}\text{Na}$ -MRI. In this example, the  $^1\text{H}$ -MRI (which is weighted by tissue T1 values) is used not only for image overlay of the  $^{23}\text{Na}$ -MRI but also as a weighted-mask, in which the T1-weighted  $^1\text{H}$ -MRI and the subtracted tissue sodium image are multiplied to yield a new sodium map, in which free fluid (and, in particular, necrotic regions) is suppressed by the combined effects of T1-weighted hyperintensity as well as reduced surviving signal on the dual-echo  $^{23}\text{Na}$ -MRI-weighted subtraction image. In this example, peripheral sodium signal encircling the necrotic core is clearly depicted. The eventual clinical utility of such approaches remains to be explored.

Limitations of the  $^{23}\text{Na}$ -MRI approach for estimating sodium concentrations in the pediatric brain include, but are not limited to, the time of imaging, with each of the dual TE sodium sequences needing  $\sim 10$  minutes, leading to a total acquisition time of  $\sim 20$  minutes, rendering data collection in children somewhat challenging without sedation. Acceleration techniques and yet-shorter TE acquisitions offer some promise for development.



Generally, the much lower sodium concentrations in the brain compared with  $^1\text{H}$  nuclei limit the use to at least 3T, with further studies needed to optimize (and thus realize the theoretic benefits of) implementation at higher field strengths, such as 7T. Currently, the postprocessing methods discussed above make a valuable contribution toward suppression of free fluid; however, complete specificity for intracellular-versus-extracellular sodium warrants further development.

## CONCLUSIONS

The technological advancements with improved pulse sequences and reconstruction methods allow combatting the challenges of measuring sodium concentrations in the pediatric brain. The sodium signal is a naturally inherent signal that does not require exogenous tracers or ionizing radiation, and in pediatric brain tumors, it is reflective of the cellular physiology of neoplastic cells in the tumor microenvironment. Here we present detailed imaging approaches to quantifying sodium concentrations in the pediatric brain that can be assessed in various CNS pathologies, with the focus on brain tumors. Future applications of  $^{23}\text{Na}$ -MRI include biopsy guidance with thresholding of the sodium concentrations to visualize potential regions of tumor with the highest mitotic activity. The major advantage of using  $^{23}\text{Na}$ -MRI will likely be to answer the complex questions on  $^1\text{H}$ -MRI that arise in monitoring treatment of pediatric patients with brain tumors: Is there residual or recurrent tumor, differentiating tumor progression versus treatment-related changes (pseudoprogression), and, in some cases at presentation, differentiating between a neoplastic process versus another mimicking pathology such as demyelinating disease.

**Disclosure forms** provided by the authors are available with the full text and PDF of this article at [www.ajnr.org](http://www.ajnr.org).

## REFERENCES

- Bottomley PA. **Sodium MRI in man: technique and findings.** In: Harris RK, ed. *Encyclopedia of Magnetic Resonance*. John Wiley & Sons, Ltd; 2007
- Gast LV, Platt T, Nagel AM, et al. **Recent technical developments and clinical research-applications of sodium ( $^{23}\text{Na}$ ) MRI.** *Prog Nucl Magn Reson Spectrosc* 2023;138-139:1-51 [CrossRef Medline](#)
- Deen SS, Riemer F, McLean MA, et al. **Sodium MRI with 3D-cones as a measure of tumour cellularity in high grade serous ovarian cancer.** *Eur J Radiol Open* 2019;6:156-62 [CrossRef Medline](#)
- Gerhalter T, Gast LV, Marty B, et al.  **$^{23}\text{Na}$  MRI depicts early changes in ion homeostasis in skeletal muscle tissue of patients with Duchenne muscular dystrophy.** *J Magn Reson Imaging* 2019; 50:1103-13 [CrossRef Medline](#)
- Schepkin VD. **Sodium MRI of glioma in animal models at ultrahigh magnetic fields.** *NMR Biomed* 2016;29:175-86 [CrossRef Medline](#)
- LaVerde G, Nemoto E, Jungreis CA, et al. **Serial triple quantum sodium MRI during non-human primate focal brain ischemia.** *Magn Reson Med* 2007;57:201-05 [CrossRef Medline](#)
- Huhn K, Engelhorn T, Linker RA, et al. **Potential of sodium MRI as a biomarker for neurodegeneration and neuroinflammation in multiple sclerosis.** *Front Neurol* 2019;10:84 [CrossRef Medline](#)
- Madelin G, Regatte RR. **Biomedical applications of sodium MRI in vivo.** *J Magn Reson Imaging* 2013;38:511-29 [CrossRef Medline](#)
- Grapperon AM, Ridley B, Verschuere A, et al. **Quantitative brain sodium MRI depicts corticospinal impairment in amyotrophic lateral sclerosis.** *Radiology* 2019;292:422-28 [CrossRef Medline](#)
- Boada FE, Qian Y, Nemoto E, et al. **Sodium MRI and the assessment of irreversible tissue damage during hyper-acute stroke.** *Transl Stroke Res* 2012;3:236-45 [CrossRef Medline](#)
- Regnery S, Behl NG, Platt T, et al. **Ultra-high-field sodium MRI as biomarker for tumor extent, grade and IDH mutation status in glioma patients.** *Neuroimage Clin* 2020;28:102427 [CrossRef Medline](#)
- Ouwertkerk R, Bleich KB, Gillen JS, et al. **Tissue sodium concentration in human brain tumors as measured with  $^{23}\text{Na}$  MR imaging.** *Radiology* 2003;227:529-37 [CrossRef Medline](#)
- Bhatia A, Lee VK, Qian Y, et al. **Quantitative sodium ( $^{23}\text{Na}$ ) MRI in pediatric gliomas: initial experience.** *Diagnostics (Basel)* 2022; 12:12232 [CrossRef Medline](#)
- Thulborn KR, Davis D, Adams H, et al. **Quantitative tissue sodium concentration mapping of the growth of focal cerebral tumors with sodium magnetic resonance imaging.** *Magn Reson Med* 1999; 41:351-59 [CrossRef](#)
- Guan G, Zhao M, Xu X, et al. **Abnormal changes in voltage-gated sodium channels subtypes NaV1.1, NaV1.2, NaV1.3, NaV1.6 and CaM/CaMKII pathway in low-grade astrocytoma.** *Neurosci Lett* 2018;674:148-55 [CrossRef Medline](#)
- Gieryng A, Pszczolkowska D, Walentynowicz KA, et al. **Immune microenvironment of gliomas.** *Lab Invest* 2017;97:498-518 [CrossRef Medline](#)
- Liberti MV, Locasale JW. **The Warburg effect: how does it benefit cancer cells?** *Trends Biochem Sci* 2016;41:211-18 [CrossRef Medline](#)
- Scharping NE, Delgoffe GM. **Tumor microenvironment metabolism: a new checkpoint for anti-tumor immunity.** *Vaccines (Basel)* 2016;4:46 [CrossRef Medline](#)
- Cong D, Zhu W, Kuo JS, et al. **Ion transporters in brain tumors.** *Curr Med Chem* 2015;22:1171-81 [CrossRef Medline](#)
- Rotoli D, Cepas MM, Maeso MD, et al. **The Na, K-ATPase  $\beta$ -subunit isoforms expression in glioblastoma multiforme: moonlighting roles.** *Int J Mol Sci* 2017;18:2369 [CrossRef Medline](#)
- Biller A, Badde S, Nagel A, et al. **Improved brain tumor classification by sodium MR imaging: prediction of IDH mutation status and tumor progression.** *AJNR Am J Neuroradiol* 2016;37:66-73 [CrossRef Medline](#)
- Schepkin VD, Ross BD, Chenevert TC, et al. **Sodium magnetic resonance imaging of chemotherapeutic response in a rat glioma.** *Magn Reson Med* 2005;53:85-92 [CrossRef Medline](#)
- Wilferth T, Gast L, Lachner S, et al. **X-Nuclei MRI on a 7T MAGNETOM Terra: initial experiences.** *MAGNETOM Flash* 2020;76
- Du J, Bydder M, Takahashi AM, et al. **Short T2 contrast with three-dimensional ultrashort echo time imaging.** *Magn Reson Imaging* 2011;29:470-82 [CrossRef Medline](#)
- Bydder M, Ali F, Saucedo A, et al. **A study of 3D radial density adapted trajectories for sodium imaging.** *Magn Reson Imaging* 2021;83:89-95 [CrossRef Medline](#)
- Feng L. **Golden-angle radial MRI: basics, advances, and applications.** *J Magn Reson Imaging* 2022;56:45-62 [CrossRef Medline](#)
- Qian Y, Panigrahy A, Laymon CM, et al. **Short-T2 imaging for quantifying concentration of sodium ( $^{23}\text{Na}$ ) of bi-exponential T2 relaxation.** *Magn Reson Med* 2015;74:162-74 [CrossRef Medline](#)
- Wilferth T, Gast LV, Stobbe RW, et al.  **$^{23}\text{Na}$  MRI of human skeletal muscle using long inversion recovery pulses.** *Magn Reson Imaging* 2019;63:280-90 [CrossRef Medline](#)
- Stobbe R, Boyd A, Smyth P, et al. **Sodium intensity changes differ between relaxation- and density-weighted MRI in multiple sclerosis.** *Front Neurol* 2021;12:693447 [CrossRef Medline](#)
- Blunck Y, Josan S, Taqdees SW, et al. **3D-multi-echo radial imaging of  $^{23}\text{Na}$  (3D-MERINA) for time-efficient multi-parameter tissue compartment mapping.** *Magn Reson Med* 2018;79:1950-61 [CrossRef Medline](#)
- Blunck Y, Kolbe SC, Moffat BA, et al. **Compressed sensing effects on quantitative analysis of undersampled human brain sodium MRI.** *Magn Reson Med* 2020;83:1025-33 [CrossRef Medline](#)
- Schramm G, Filipovic M, Qian Y, et al. **Resolution enhancement, noise suppression, and joint T2\* decay estimation in dual-echo**

- sodium-23 MR imaging using anatomically guided reconstruction. *Magn Reson Med* 2024;91:1404–18 [CrossRef Medline](#)
33. De Leon-Benedetti L, Narayanan S, Lee VK, et al. **The use of sodium MRI in the diagnosis of an anaplastic astrocytoma during immunotherapy: a case report.** *Childs Nerv Syst* 2024;40:965–67 [CrossRef Medline](#)
  34. Pahor M, Manini MC. **High resolution sodium imaging of human brain at 7T.** *Bone* 2008;23:1–7
  35. Huang L, Bai J, Zong R, et al. **Sodium MRI at 7T for early response evaluation of intracranial tumors following stereotactic radiotherapy using the CyberKnife.** *AJNR Am J Neuroradiol* 2022;43:181–87 [CrossRef Medline](#)
  36. Nunes Neto LP, Madelin G, Sood TP, et al. **Quantitative sodium imaging and gliomas: a feasibility study.** *Neuroradiology* 2018; 60:795–802 [CrossRef Medline](#)
  37. Nagel AM, Bock M, Hartmann C, et al. **The potential of relaxation-weighted sodium magnetic resonance imaging as demonstrated on brain tumors.** *Invest Radiol* 2011;46:539–47 [CrossRef Medline](#)